RESEARCH ARTICLE | MARCH 30 2023

Precessing cylinder as high-shear-rate mixer: Application to emulsification

Special Collection: Precession, Nutation, and Libration Driven Flows

Susumu Goto ; Yasufumi Horimoto ; Takuro Kaneko ; Kohei Oya ; Yuji Sugitani ; Shota Aritsu ; Masato Yoshida ; Haruka Ohyama ; Kento Eguchi ; Shota Kukimoto ; Kazuo Matsuyama ; Toru Nishimura ; Kimikazu Fukuda ; Keiichi Onoda

Physics of Fluids 35, 035139 (2023)
https://doi.org/10.1063/5.0139991

Physics of Fluids ARTICLE scitation.org/journal/phf

Precessing cylinder as high-shear-rate mixer: Application to emulsification

Cite as: Phys. Fluids **35**, 035139 (2023); doi: 10.1063/5.0139991
Submitted: 26 December 2022 · Accepted: 27 February 2023 ·
Published Online: 30 March 2023

Susumu Goto,[1,a] Yasufumi Horimoto,[2] Takuro Kaneko,[1] Kohei Oya,[1] Yuji Sugitani,[1] Shota Aritsu,[1] Masato Yoshida,[1] Haruka Ohyama,[1] Kento Eguchi,[1] Shota Kukimoto,[1] Kazuo Matsuyama,[3] Toru Nishimura,[4] Kimikazu Fukuda,[4] and Keiichi Onoda[4]

AFFILIATIONS

[1]Graduate School of Engineering Science, Osaka University, 1-3 Machikaneyama, Toyonaka, Osaka 560-8531, Japan
[2]Laboratory for Flow Control, Faculty of Engineering, Hokkaido University, Sapporo, Hokkaido 060-8628, Japan
[3]Open Innovation Institute, Kyoto University, Kyoto-daigaku-katsura, Nishikyo, Kyoto 615-8530, Japan
[4]R&D, Processing Development Research, Kao Corporation, Minato, Wakayama 640-8580, Japan

Note: This paper is part of the special topic, Precession, Nutation, and Libration Driven Flows.
[a]**Author to whom correspondence should be addressed:** s.goto.es@osaka-u.ac.jp

ABSTRACT

Through laboratory experiments of oil-in-water emulsification, we show that we can construct a high-shear-rate mixer (precession mixer) by using the precession of a cylindrical container without any mixing blades. For high-shear-rate mixing, a container with a larger diameter and its faster spin are preferable so that the wall velocity becomes large enough. Then, emulsification is most efficient when we set the Poincaré number $Po = \Omega_p/\Omega_s$, which is the ratio of the spin and precession rotation speeds, about 0.2–0.3. When Po is smaller than these values, shear rates in the mixer get much lower, though mixing in the bulk of the container is enhanced. On the other hand, when Po is larger, shear rates near the cylindrical wall get higher but mixing in the bulk drastically declines. Through our systematic parameter survey for efficient emulsification by the precession mixer, we have also discovered an experimental law describing the maximum shear rate in the mixer. Since we can use it to appropriately choose the driving conditions of the mixer according to the properties of the materials to be mixed, this experimental law gives useful information for the practical use of the mixer.

I. INTRODUCTION: PRECESSING CONTAINER AS A MIXER

Mixing is one of the most important processes in a wide variety of industries. In most of conventional mixers, blades drive flow and mixing. However, collision with rapidly rotating blades or high shear rates around them can damage materials to be mixed. This is disadvantageous in the cases that require delicate mixing in bioengineering, food processing, pharmaceutical industries, and so on. In addition, mixers with blades with complex structures require careful cleaning, and it sometimes leads to significant loss of mixed materials. It is, therefore, desirable to construct a bladeless mixer with a smoothly shaped container.

A simple method to drive flow is the rotation of a container. However, flow of a fluid filled in a container that rotates at a constant angular velocity, irrespective of the container's shape, always tends to the solid-body rotation (p. 7 of Ref. 1). This spin-up process (p. 35 in Ref. 1) rapidly weakens the mixing ability of the flow. Therefore, to keep the mixing ability of the rotating container, we must avoid the spin-up. Two kinds of strategies can achieve this: (i) We partially filled a fluid in a container and (ii) we change the amplitude or direction of the angular velocity vector of the spin of the container. We show in Fig. 1 some examples of bladeless mixers using these strategies. Figure 1(a) shows the so-called soft mixer,[2] which adopts the first strategy. The mixer is composed of a cylindrical vessel slightly tilted from the vertical direction, and it rotates about its axis. Even if the angular velocity is constant, because of the liquid–gas interface, which is horizontal and, therefore, it is not perpendicular to the spin axis, flow can become complex leading to mixing without high shear rates. Recently, another simple bladeless mixer was proposed by Watanabe and Goto,[3] namely, a constantly rotating sphere, which is partially filled with liquid. Again, the liquid–gas interface plays an important role leading to a pair of counter-rotating vortices whose axes are perpendicular to the spin axis of the container (see Fig. 4 of Ref. 3).

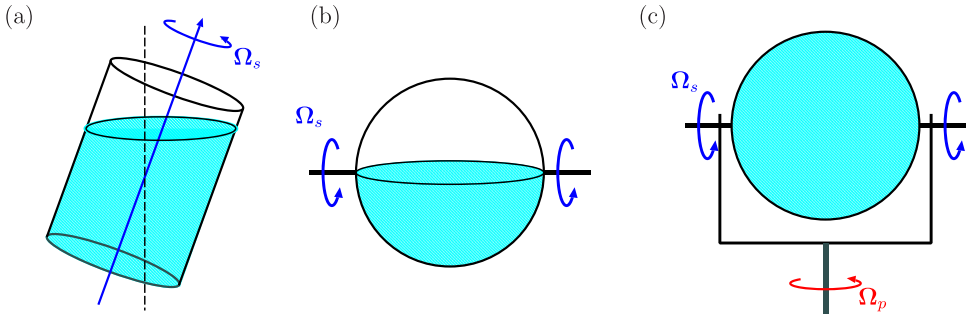

FIG. 1. Examples of bladeless mixers: (a) soft mixer,[2] a cylinder tilted from vertical with a liquid–gas interface rotating about its axis; (b) a spherical container which is partially filled with liquid rotates about the horizontal axis;[3] (c) precession mixer[4] with a spherical container, the spin axis of the rotating container filled with liquid rotates about another axis (the precession axis).

These vortices lead to permanent mixing in the container even if its spin angular velocity is constant.

In the present article, we investigate the second strategy to avoid the spin-up of confined fluid in a container. More concretely, we use the precession of the spin axis. Figure 1(c) shows an example of the precession mixer, namely, a precessing spherical container. Since the spin axis is not stationary but it rotates in the laboratory frame, confined fluid cannot tend to solid-body rotational flow forever. In fact, there exist commercial mixers using the precession of the container. Although in many of them, the container is apart from the precession axis to use the centrifugal force, in the present study, we use a precession mixer in which the container's center is located at the crossing point of the precession and spin axes. In our previous study,[4] we numerically showed that a relatively slow precession [$Po \approx 0.1$; see Eq. (1) for the definition of Po] leads to rapid mixing of fluid confined in a precessing sphere. Our numerical simulations showed that only 10 spins are required by complete mixing. However, as will be shown in the following of the present article, this weak precession cannot produce high shear rates. Although this can be an advantage for the mixing of delicate materials, we have been conducting laboratory experiments to investigate whether or not the precession mixer is also useful for mixing such as emulsification, which requires high shear rates. In this article, we show the experimental evidence that this is indeed the case.

Once we fix the container's shape and the angle between the spin and precession axes, flow in a precessing container depends on two non-dimensional parameters. In the present study, we restrict ourselves in the case that (i) the container is cylindrical, (ii) the spin axis and precession axis are perpendicular, and (iii) the precession axis is horizontal [Fig. 2(a)]. Then, the first control parameter is the Poincaré number,

$$Po = \frac{\Omega_p}{\Omega_s}, \tag{1}$$

which is the ratio between the precession rotation speed Ω_p and the spin rotation speed Ω_s, and the other is the Reynolds number,

$$Re = \frac{A^2 \widetilde{\Omega}_s}{\nu}, \tag{2}$$

where A is the characteristic length of the container (in the present study, we adopt the radius, $D/2$, of the cylindrical container with diameter D), ν is the kinematic viscosity of confined fluid, and $\widetilde{\Omega}_s = 2\pi\Omega_s$ is the spin angular velocity. One of the most important characteristics of flow in a precessing container is that flow states drastically change with Po (Refs. 4, 5, and 6). For sufficiently weak precession, $Po \ll 1$, a steady global circulation whose rotational axis is a little inclined from the spin axis of the container is sustained.[7–12] When we fix Re at a sufficiently large value [i.e., $Re \gtrsim O(10^4)$] and we increase Po, the steady flow becomes unstable[13–19] and bulk turbulence occurs at $Po = O(10^{-2})$ (Refs. 20–22) (see also Refs. 23 and 24 for details of the low-Po transitions). The precise critical Po for turbulence to be sustained depends on the shape of the container; for example, a spherical container requires smaller Po to sustain turbulence than a spheroidal one because the normal stress on the spheroidal container's wall can stabilize the circulation about the spin axis.[25] When $Po \approx 0.1$, most developed turbulence is sustained in the bulk of the flow irrespective of the container's shape and most rapid mixing occurs.[4] However, for larger Po, the flow in the bulk tends to follow the rotation with $\boldsymbol{\Omega}_p$ ($= \Omega_p \boldsymbol{e}_p$), where $\boldsymbol{e}_p$ is the unit vector parallel to the precession axis, because the precession axis is stationary in

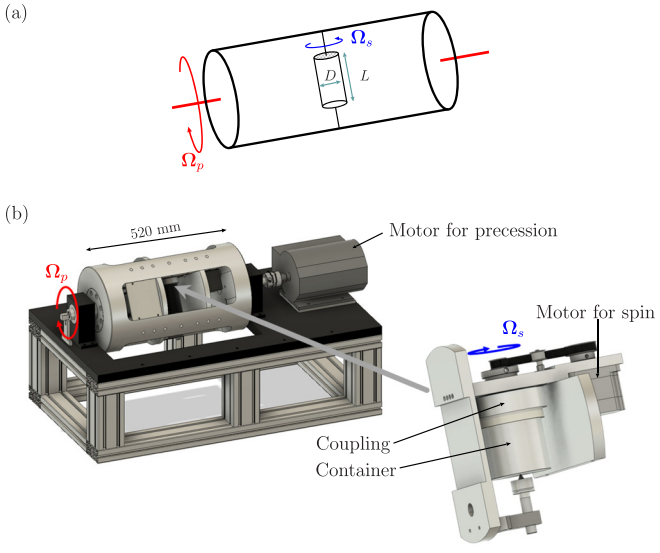

FIG. 2. (a) Schematic of a precessing cylindrical container with diameter D and length L, which spins at $\boldsymbol{\Omega}_s$ in a rotating drum. We call the frame fixed in the drum the precession frame, which rotates at $\boldsymbol{\Omega}_p$ with respect to laboratory. (b) Precession mixer used in the present study. The driving unit of spin of the cylindrical container is installed in the aluminum drum with diameter 300 mm and axial length 520 mm, which rotates about its horizontal axis at $\boldsymbol{\Omega}_p$. The spin axis and the precession axis cross at the center of the container.

laboratory frame. In fact, when Po is larger than about 0.2, the bulk flow may be approximated by the rotation at $\mathbf{\Omega}_p$ with respect to the laboratory frame. In other words, the fluid in the bulk is approximately still in the precession frame, which is the frame rotating at $\mathbf{\Omega}_p$, while the container spins with $\mathbf{\Omega}_s$ ($= \Omega_s \boldsymbol{e}_s$). Here, $\boldsymbol{e}_s$ is the unit vector parallel to the spin axis. Therefore, if Ω_s is sufficiently large, then there exists a boundary layer near the container's wall with high shear rates. It is this shear layer created without blades that we use for emulsification. In the following, we show that the precession mixer can be used even in the cases requiring high shear rates.

II. EXPERIMENTAL METHODS

A. Apparatus

We have been developing several precession mixers (Appendix A) to investigate the possibility of high-shear-rate mixing. As described in Sec. I, we need larger Po defined by Eq. (1), i.e., larger Ω_p, for such mixing. In order to conduct experiments with large Ω_p, we construct the apparatus shown in Fig. 2. In this apparatus, we use an aluminum drum with sufficient inertia (diameter 300 mm and axial length 520 mm) for stable rotation about the horizontal precession axis. This rotation is driven by a motor (Hitachi, TFO-LK 2P 1.5 kW) up to about $\Omega_p = 1500$ rpm. In the drum, we set a container, a stepper motor (Oriental Motor, PKE596AC) whose step angle is 0.72°, its driver, and a small PC (Raspberry Pi model 3B+), which we use as an accurate pulse generator. We can set a cylindrical container with diameter D smaller than about 150 mm, and the maximum spin rate is about $\Omega_s = 5000$ rpm. These wide ranges of parameters ($\Omega_s \lesssim 5000$ rpm, $\Omega_p \lesssim 1500$ rpm, and $D \lesssim 150$ mm) enable us to conduct a systematic parameter survey for exploration of the possibility of high-shear-rate mixing.

B. Containers

We use four cylindrical containers with different diameters and lengths (depths); see Table I. Since, as will be shown in Secs. III and IV, the diameter of the container is an important parameter, which controls shear rates, we examine three diameters $D = 29$, 58, and 87 mm. In contrast, to show that the axial length of the container is unimportant, we examine two lengths 52 and 104 mm for a common D ($= 58$ mm).

We report, in Sec. III, results with the spin of $\Omega_s \leq 4000$ rpm and precession of $\Omega_p \leq 1200$ rpm. Since the precession requires the force acting on the spin axis, which is proportional to Ω_s and Ω_p and the moment of inertia of the container, the strength of the spin axis limits the range of Ω_s and Ω_p for larger containers. We examine ten cases with different combinations of Ω_s and Ω_p for container D29L52, 31 cases for D58L52, eight cases for D58L104, and four cases for D87L104.

TABLE I. Containers used in the present experiments. We examine mixing in four cylindrical containers with three different diameters and two different lengths of the cavity.

Container	Diameter, D (mm)	Length, L (mm)
D29L52	29	52
D58L52	58	52
D58L104	58	104
D87L104	87	104

C. Examined process

To explore the possibility of high-shear-rate mixing, we examine an oil-in-water emulsification process. More concretely, we use water with 0.5 wt % polyvinyl alcohol (Mitsubishi Chemical, EG-05) as the continuous phase and cyclic dimethyl silicon (Shin-Etsu Silicones, KF-96A-6cs) as the dispersed phase. The weight ratio of the continuous and dispersed phases is 4:1. This sample is advantageous for our purpose because (i) the diameter of produced droplets is only weakly affected by the temperature and (ii) the produced droplets are quite stable and we can repeatedly measure their diameters after the production process (see Fig. 3 and Ref. 26). Thanks to the former property, we conduct the experiments in a room whose temperature is controlled at 20 °C, but we do not conduct further accurate temperature control of the working fluid. Incidentally, because of the energy dissipation during the mixing, the temperature of the fluid increases with about 15 °C at most.

The concrete process procedure is as follows: We prepare in advance the continuous phase with sufficient mixing. First, we pour it into the container and then add the oil so that the total filling ratio can be 90%; since the container does not have an air vent hole, we cannot fill it with liquid. After setting a rubber lid, we connect the container with the spin axis through the coupling shown in Fig. 2. We start driving both the spin and precession simultaneously with an acceleration period of 10 s. Then, we keep the precession for the mixing time T (s). The deceleration period is about 90 s.

D. Estimation of droplet diameter

In this subsection, we explain the method to measure the diameter of the produced oil droplets. Our measurements are simple relying on the image analysis of their rising process; since smaller droplets rise slower, we can estimate their diameter from the rising velocity. The concrete procedures are as follows.

First, we pour the produced emulsion, after a gentle mixing by hand for uniform dispersion of droplets, into acrylic cylindrical vessels with a diameter of 16 mm and height of 330 mm. We can simultaneously measure the rising velocity with two, four, and nine vessels for a single mixing process with containers D58L52, D58L104, and D87L104, respectively (Table I), while we repeat the mixing twice with the smallest container, D29L52, for a single measurement of the rising velocity so that we can prepare sufficient amount of emulsion.

We set a white light-emitting diode (LED) sheet behind the cylinders and record images every 5 s by a digital camera (Basler, acA1920–150um) for the time duration, which depends on the rising velocity of droplets, between 3600 and 43 200 s.

We show, in Fig. 3(a), examples of cropped images of the taken pictures in the case of $\Omega_s = 2000$ rpm and $\Omega_p = 800$ rpm with container D58L52. We show two time-series for 10 800 s recorded on different days: One is just after the production of the emulsion, and the other is 12 days later. We define the bottom interface of the emulsion, which corresponds to brighter regions in Fig. 3(a), by analyzing these images. Note that since the coalescence of droplets hardly occurs, the rise in the bottom interface corresponds to that of droplets with a representative size. Figure 3(b) shows the binarized images. Here, we use the threshold of the brightness as αB (with $\alpha = 0.9$) with B being the initial brightness of the image of the emulsion. Then, we can identify

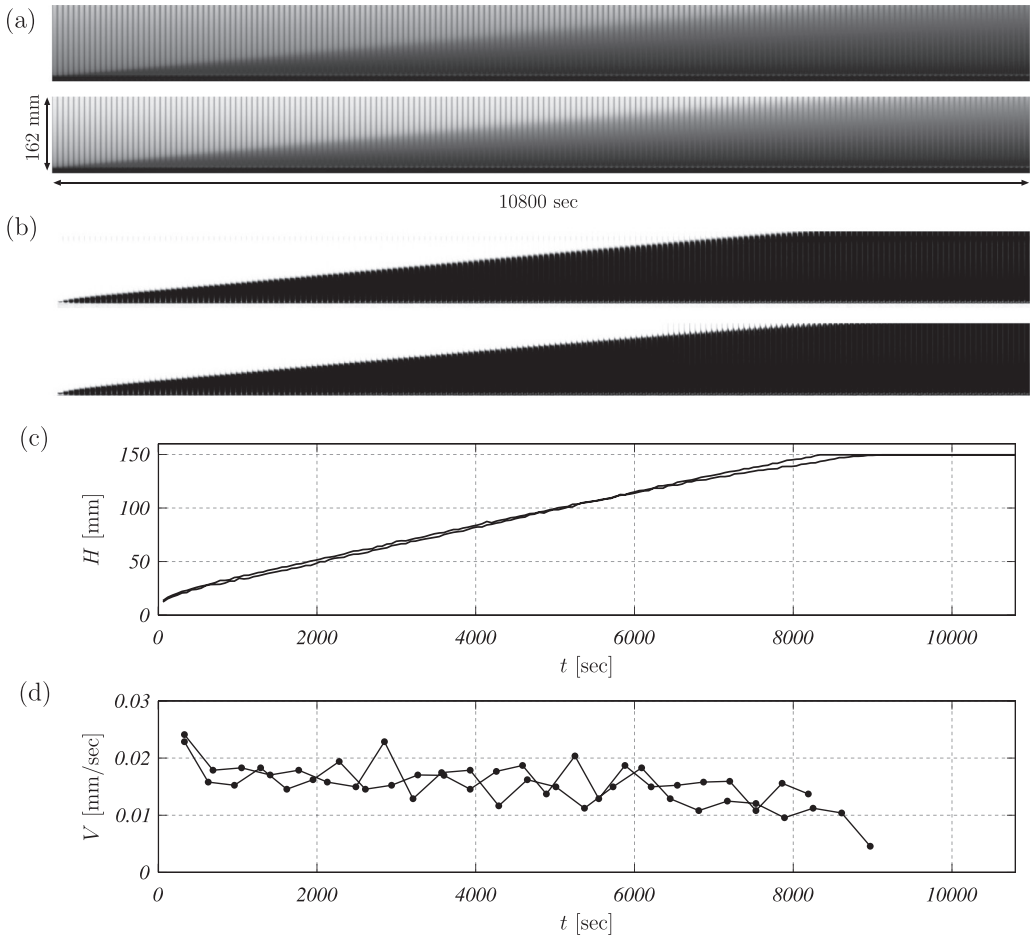

FIG. 3. Example of the estimation of the representative diameter of produced droplets. Parameters are $\Omega_s = 2000$ rpm, $\Omega_p = 800$ rpm, and $T = 400$ s. (a) Time-elapsed images of emulsion in a cylindrical vessel. Two series of images are taken on different days (one is the same day of the emulsification, and the other is 12 days later) by using the same product. (b) Binarized images. (c) The temporal evolution of the height H of the emulsion interface; the two curves correspond to the two time-series shown in (a) and (b). (d) The rising velocity of the emulsion estimated by the moving average of the time derivative of H.

the height H of the interface as a function of time [Fig. 3(c)]. Incidentally, the estimated rising velocity depends on the choice of threshold α because smaller values of α capture the motion of smaller droplets. However, since we are interested in the largest size of droplets, we fix α at a large value ($\alpha = 0.9$). We have also confirmed that the dependence of the results on α in the range $\alpha \in [0.85, 1]$ is negligibly small in the examined cases.

By taking the time derivative of the height of the interface, we can estimate the typical rising velocity V of the emulsion. We show the velocity V, which is obtained by the moving average, in Fig. 3(d), for example. Since the rising velocity gets slower as time elapses probably because of the finite height of the cylinder for the measurements [see Fig. 9(b) in Appendix B], we take the average of V in the steadily rising stage. On the other hand, the rising velocity V_s of a single droplet with diameter d is estimated by

$$V_s = \frac{(\rho - \rho')\, d^2\, g}{18\mu} \tag{3}$$

under the assumption that the buoyancy and the Stokes drag are balanced. In Eq. (3), ρ, ρ', μ, and g denote the mass density of water and oil, the viscosity of water, and the gravitational acceleration, respectively. Then, we further assume $V \approx V_s$ to estimate the droplet diameter d. Thus, the estimated diameter is a representative of distributed diameters of droplets. Incidentally, we have confirmed that the Sauter mean diameter measured by the laser diffraction method is approximately proportional to the diameter estimated by our method (Appendix C). It is also important to observe in Fig. 3 that the two measurements conducted on two different days lead to almost identical results. This is direct evidence of the stability of the produced emulsion. As mentioned in Sec. II C, since the droplets are quite stable once they are created, we can repeat the procedure mentioned in this subsection for a single product. Besides, we can simultaneously measure the rising velocities, by using several cylindrical vessels, for different mixing parameters because the state of emulsion is independent of their ages. This property is useful for the accurate estimation of droplet diameter.

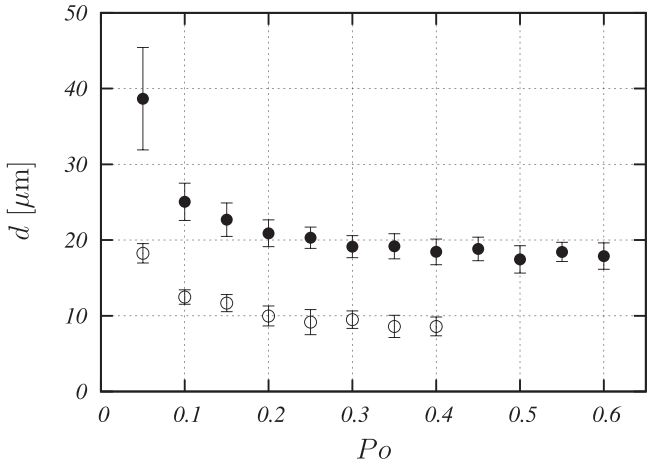

FIG. 4. Representative diameter d of oil droplets as functions of Po. The emulsion is produced by using container D58L52 with fixed values of Ω_s at 2000 rpm (•) and 3000 rpm (○). The error bars indicate the standard deviation, which is averaged over the samples, due to the temporal variations of the rising velocity of droplets.

III. RESULTS

A. *Po*-dependence for fixed *Re*

In this section, we show results on the estimation of the produced droplets' diameter under different mixing conditions. First, we examine the dependence on the precession rotation speed Ω_p for a fixed value of Ω_s by using a container (D58L52). This corresponds to the examination of the dependence on the Poincaré number Po, defined by Eq. (1), for a fixed value of the Reynolds number Re, defined by Eq. (2).

As described in Sec. I, the flow states drastically depend on Po. Accordingly, the diameter of the produced emulsion also strongly depends on Po. We show its evidence in Fig. 4, where we show results with container D58L52 for two fixed values of the spin rotation speed: $\Omega_s = 2000$ rpm (closed circles) and 3000 rpm (open circles). For these experiments, we change the precession rotation speed in the range $\Omega_p \leq 1200$ rpm to show the estimated diameter d of produced droplets as functions of Po ($= \Omega_p/\Omega_s$). In Fig. 4, we show the results with the mixing time $T = 480$ s since the estimated diameter only slightly changes even if we make T twice longer (see Appendix B).

Here, it is worth mentioning the relationship between Ω_s and Re. Although it is difficult to estimate or accurately measure the kinematic viscosity ν of the working fluid, we have measured it by Brookfield viscometer to confirm that $\nu = O(10^{-6})$ m^2/s even after the emulsification. Then, the Reynolds number is about $Re = O(10^5)$ for these values of Ω_s (2000 and 3000 rpm), which is high enough for the shear rate in the boundary layer on the container's sidewall to be high (see Sec. IV). Incidentally, even when we use the smallest container (D29L52), Re is always lager than 10^4 for all the examined parameters.

It is evident in Fig. 4 that the diameter d of droplets is a decreasing function of Po when Re is fixed. We recall (see Sec. I) that the most developed turbulence is sustained in the bulk of the container when $Po \approx 0.1$. In other words, the shear rate in the bulk turbulence (sustained when $Po \approx 0.1$) is not responsible for the emulsification. It is the high shear rates near the wall (sustained for larger Po) that enhance the emulsification. Looking at Figs. 5–9 in Ref. 6, we notice that there is a drastic change in the flow state in the bulk; it is highly turbulent when $Po = 0.1$, whereas it is quiescent when $Po = 0.4$. We emphasize that in such a case with higher Po, there exists thin shear layer near the rotating wall with velocity $D\widetilde{\Omega}_s/2$. In fact, Fig. 4 shows that d decreases when Po increases from 0.05 to 0.2. We also observe that d seems to tend to a constant value when $Po \gtrsim 0.2$.

Precisely speaking, d depends on Po in a large Po range because the boundary layer thickness is proportional to $Po^{-1/2}$ (see Ref. 27) and the shear rate near the wall increases with Po. However, in practice, it is not realistic to drive the system with large Po for two reasons. One is the safety reason, i.e., it is dangerous to rotate the system with large Ω_p. The other reason is the mixing time. As discussed in Appendix B, the bulk flow for large Po cannot be mixed well. This implies that there is an optimal value of Po when we mix the materials within reasonable time. Therefore, we examine, in the following, the cases with fixed Po at 0.2 and 0.3.

B. Dependence on *Re*, *D*, and *L* for fixed *Po*

We have shown in Sec. III A that the Poincaré number, Po, is an important parameter to determine shear stress in the precession mixer. More precisely, for fixed Ω_s in a common container, precession with

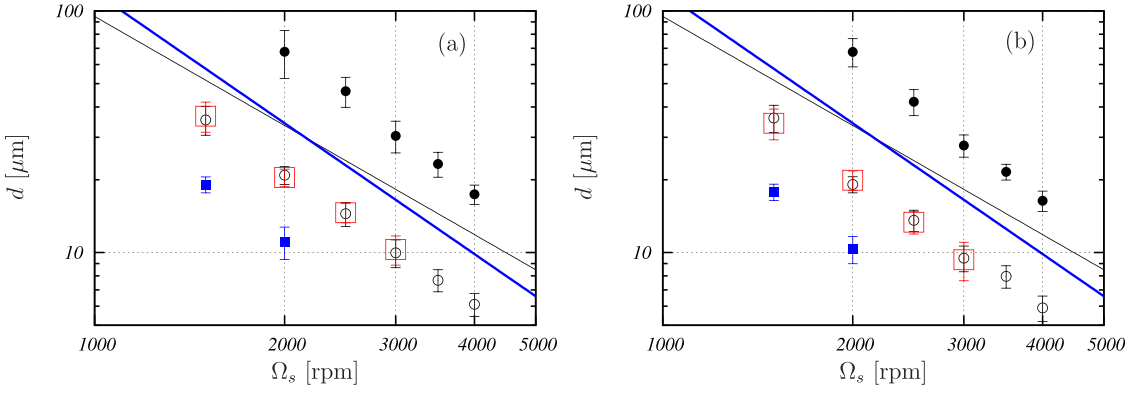

FIG. 5. Representative diameter d as a function of Ω_s for a fixed Po at (a) 0.2 and (b) 0.3. Different symbols denote the results with different containers: •—D29L52; ○—D58L52; □—D58L104; ■—D87L104. The black and blue straight lines indicate $\Omega_s^{-1.5}$ and $\Omega_s^{-1.8}$, respectively.

larger Po produces higher shear rates and therefore stronger shear stress. In practice, however, $Po \approx 0.2$–0.3 is sufficient for effective emulsification (Fig. 4); in fact, larger Po leads to higher shear rates, but the mixing time gets longer (Appendix B).

Therefore, in this subsection, we investigate how the droplet diameter depends on the spin rotation speed Ω_s and the container size (i.e., D and L). We show in Fig. 5 the Ω_s-dependence of the representative diameter d of droplets for (a) $Po = 0.2$ and (b) 0.3. Different symbols in the plots denote results with different containers.

First, let us see the results with a common container, for example, the open circles for D58L52. It is evident that the droplet diameter d monotonically decreases as Ω_s increases. As will be discussed in Sec. IV, this implies that the shear rate increases with Ω_s. Since Fig. 5 is a logarithmic plot, the straight lines indicate power-law dependence of d on Ω_s. The experimental results are well fitted by the scaling $d \sim \Omega_s^{-\gamma}$ with $\gamma \approx 1.8$, which is indicated by the blue line.

Next, looking at the results for the D58L52 (open circles) and those with D58L104 (red open squares) in Fig. 5, we notice that the axial length (i.e., aspect ratio) of the cylindrical container does not affect the droplet diameter. In other words, the shear stress, for fixed Po, is determined by the rotation speed Ω_s and container diameter D and it is independent of L. This result is consistent with the picture (see Sec. IV) that the emulsification occurs in the thin boundary layer near the sidewall of the cylindrical container.

It is of interest to observe that the droplet diameter d depends on the diameter D of the container for fixed Ω_s and Ω_p. More precisely, comparing the results with D29L52 (closed circles), D58L52 (open circles), and D87L104 (blue closed squares), fatter containers produce smaller droplets for fixed rotation conditions. This implies that the larger diameter of the container can sustain the higher shear rate near the cylindrical wall because wall velocity is larger for larger D for fixed Ω_s in the precession frame. More quantitative arguments will be given in Sec. IV.

IV. DISCUSSION

In this section, we estimate the size of droplets produced by the precession mixer. First, we assume that the boundary layer thickness δ on the sidewall of the cylindrical container is scaled by

$$\delta \sim D\,Re^{-\beta} \tag{4}$$

for a fixed value of Po. Here, D is the diameter of the container, Re is the Reynolds number defined by Eq. (2), and β (>0) is a constant. Although it is known[7,10] that $\beta = 1/2$ for the Ekman layer in weakly precessing containers (i.e., $Re \gg 1$ and $Po \ll 1$), it is difficult to theoretically predict β for $Po = O(0.1)$, which is the range of Po examined in the present experiments. Incidentally, Pizzi *et al.*[28] numerically estimated δ in a precessing cylinder with $2 \times 10^3 \le Re \le 10^4$ and $Po = O(0.1)$ to compare its scaling with the Stewartson layer ($\beta = 1/4$), but the scaling is not conclusive.

Here, we reemphasize that for $Po \gtrsim 0.2$, the flow in the bulk is almost still in the precession frame, while the container's wall moves with the velocity $\pi D \Omega_s$. Then, we may estimate the shear rate on the wall as

$$\dot{\gamma} \sim \frac{D\Omega_s}{\delta} \sim \Omega_s\, Re^{\beta} \sim \nu^{-\beta}\, D^{2\beta}\, \Omega_s^{1+\beta}, \tag{5}$$

and, therefore, the shear stress $\tau = \rho\,\nu\,\dot{\gamma}$ as

$$\tau \sim \rho\,\nu^{1-\beta}\, D^{2\beta}\, \Omega_s^{1+\beta}. \tag{6}$$

Since we can estimate the maximum diameter $d_{\max}$ of droplets by the balance between τ and $\sigma/d_{\max}$ with σ being the surface tension, we obtain

$$d_{\max} \sim \frac{\sigma}{\rho\,\nu^{1-\beta}\, D^{2\beta}\, \Omega_s^{1+\beta}} \quad (\text{for fixed } Po \gtrsim 0.2). \tag{7}$$

The above estimation (7) implies that the droplet size is smaller for a larger spin rotation speed Ω_s and for larger diameter D of the container. This is consistent with the experimental results shown in Fig. 5.

If we use the exponent, $\beta = 1/2$, for the Ekman layer, then Eq. (7) leads to the scaling, $d_{\max} \sim \Omega_s^{-3/2}$, which does not explain the experimental data shown in Fig. 5; see the black line. Instead, we heuristically choose the value of β as $\beta = 0.8 (= 4/5)$ in the range of $Po = 0.2$–0.3 examined in our experiments. Then, Eq. (7) leads to

$$d_{\max} \sim D^{-8/5}\, \Omega_s^{-9/5} \quad (\text{for fixed } Po \approx 0.2 - 0.3). \tag{8}$$

According to the scaling (8), we rescale the results shown in Fig. 5. The results are shown in Fig. 6. We can see that Eq. (8) excellently

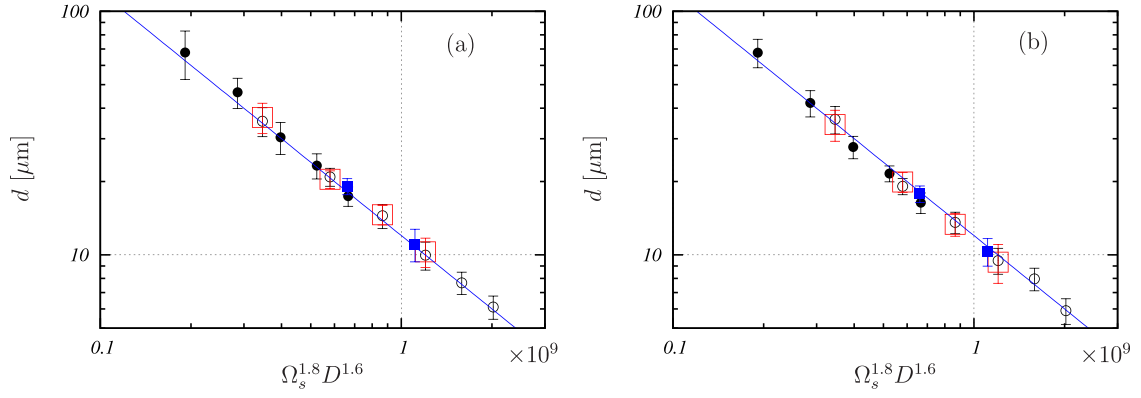

FIG. 6. We rescale the data shown in Fig. 5 according to Eq. (7) with $\beta = 0.8$. The symbols are the same as in Fig. 5. We can see that the data collapse irrespective of the containers' size: (a) $Po = 0.2$ and (b) $Po = 0.3$. The straight line indicates the power law with exponent -1.

explains all the experimental results of the droplet size. In other words, we may predict the maximum shear rate in the precession mixer as

$$\dot{\gamma} \sim D^{8/5}\,\Omega_s^{9/5} \quad (\text{for fixed } Po \approx 0.2 - 0.3). \tag{9}$$

Hence, when we desire to control the shear stress on the material to be mixed, we appropriately choose the container's diameter D and the spin rotation speed Ω_s according to this experimental law.

V. CONCLUSION

The precession mixer can drive mixing in a smooth container without using blades. One of the most advantageous characteristics of the mixer is that if we appropriately choose the driving parameters, we can avoid the damage of delicate materials due to high shear stress. However, (i) accurate estimation of shear stress on materials in the mixer was unknown. This means that we could not set the appropriate parameters for low-shear-rate mixing in the precession mixer. (ii) It was also unknown whether we could use the mixer for high-shear-rate mixing such as emulsification process. The present study has solved these issues. More concretely, we have shown that if we appropriately choose the container's size and rotation speeds, we can control the shear stress acting on materials in the mixer as we want.

Concerning the second issue (ii), we have shown that the precession mixer can produce high shear rates at the larger $Po = \Omega_p/\Omega_s$ range, $Po \gtrsim 0.2$ with larger diameter D of a container and lager spin rotation speed Ω_s. To demonstrate this, we have conducted a series of parameter studies of emulsification by using the cylindrical containers (Table I) and the precession mixer shown in Fig. 2. We emphasize again that the most important parameter to drive high-shear-rate mixing is Po. When we fix Ω_s for a container, the droplet size decreases with Po particularly in the range of $Po = 0.1$–0.2 (Fig. 4). This is because the bulk flow for $Po \gtrsim 0.2$ is quiescent in the precession frame and the rapid spin rotation creates a thin boundary layer near the side cylindrical wall. The shear rate in the layer gets higher for larger Po, which was numerically shown for a precessing sphere.[4] However, since the bulk flow gets quite slow for higher Po leading to the reduction of mixing in the bulk, the appropriate Po is around 0.2–0.3 for fixed mixing time in practice (Appendix B).

For high shear rate mixing with $Po = 0.2$–0.3, we should use a container with larger diameter D, if we fix the spin rotation speed Ω_s (Fig. 5). In fact, the representative diameter of produced droplets obeys the scaling (8). Although we derive (8) by heuristic arguments (Sec. IV) under the assumption of the scaling (4) of boundary layer thickness, it excellently explains the experimental results (Fig. 6). The fact that we can reduce the rotation speeds with larger containers is a desirable feature in practical applications for high shear rate mixing. Incidentally, in the precession mixer (Fig. 2), we use in the present study the spin and precession axes cross at the center of the container. This enables us to make the mixer compact, and it also avoids the centrifugal effects acting on the two fluids with different mass densities.

Through the present experiments of emulsification, we have also addressed issue (i). More precisely, Fig. 4 shows that the shear rate is much lower for $Po \lesssim 0.05$ than for $Po \gtrsim 0.2$. Recalling that mixing in the bulk is most rapid when $Po \approx 0.1$ (see Ref. 4), we may choose an appropriate value of Po for desirable mixing. In addition, the discovered experimental law for the shear rate (9) in the range of $Po = 0.2$–0.3 is also useful to control the shear stress in the precession mixer according to the properties of materials to be mixed.

ACKNOWLEDGMENTS

This study was partly supported by JSPS Grant-in-Aids for Scientific Research (No. 20H02068).

AUTHOR DECLARATIONS

Conflict of Interest

The authors have no conflicts to disclose.

Author Contributions

Susumu Goto: Conceptualization (lead); Data curation (equal); Formal analysis (equal); Funding acquisition (equal); Investigation (equal); Methodology (equal); Project administration (equal); Supervision (equal); Visualization (equal); Writing – original draft (lead); Writing – review & editing (equal). **Shota Kukimoto:** Data curation (equal); Formal analysis (equal); Visualization (equal); Writing – review & editing (equal). **Kazuo Matsuyama:** Conceptualization (equal); Writing – review & editing (equal). **Toru Nishimura:** Conceptualization (supporting); Writing – review & editing (equal). **Kimikazu Fukuda:** Conceptualization (supporting); Writing – review & editing (equal). **Keiichi Onoda:** Writing – review & editing (equal). **Yasufumi Horimoto:** Data curation (equal); Formal analysis (equal); Investigation (equal); Writing – review & editing (equal). **Takuro Kaneko:** Data curation (equal); Formal analysis (equal); Writing – review & editing (equal). **Kohei Oya:** Data curation (equal); Formal analysis (equal); Writing – review & editing (equal). **Yuji Sugitani:** Data curation (equal); Formal analysis (equal); Writing – review & editing (equal). **Shota Aritsu:** Data curation (equal); Formal analysis (equal); Writing – review & editing (equal). **Masato Yoshida:** Data curation (equal); Formal analysis (equal); Writing – review & editing (equal). **Haruka Ohyama:** Data curation (equal); Formal analysis (equal); Visualization (equal); Writing – review & editing (equal). **Kento Eguchi:** Data curation (equal); Formal analysis (equal); Visualization (equal); Writing – review & editing (equal).

DATA AVAILABILITY

The data that support the findings of this study are available from the corresponding author upon reasonable request.

APPENDIX A: PROTOTYPES OF THE PRECESSION MIXER

We have developed several types of the precessing mixer to investigate its abilities. Since some of driving mechanisms may be used for future applications, here we briefly describe the advantages and disadvantages of three kinds of the developed mixers (Fig. 7).

First, Fig. 7(a) shows a precession mixer, which uses a pair of bevel gears. An advantage of this mixer is that we need only a single motor to drive the spin $\boldsymbol{\Omega}_s$ and precession $\boldsymbol{\Omega}_p$. In addition, since the driving mechanism is simple, we can drive relatively high spin rotation speed. The disadvantage is that $Po = \Omega_p/\Omega_s$ is fixed. Thus, we used this precession mixer [Fig. 7(a)] to reveal the values of Ω_s needed for emulsification, but we could not show the importance of Po.

Then, next, we developed another mixer [Fig. 7(b)] so that we could change Po. A pair of miter gears and two motors enable us to

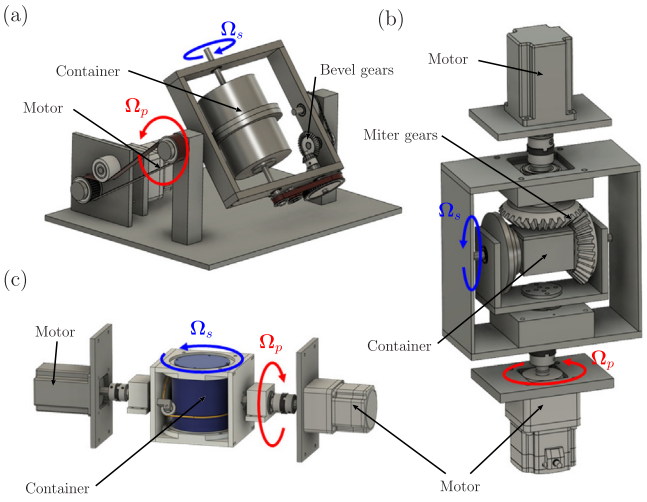

FIG. 7. Prototypes of the precession mixers. (a) By using bevel gears, we can drive the two rotations $\boldsymbol{\Omega}_s$ and $\boldsymbol{\Omega}_p$ simultaneously by a single motor for a fixed value of *Po*. (b) By using two miter gears and two motors, we can change both Ω_s and Ω_p. (c) Similar to the mixer shown in (b), we can set both Ω_s and Ω_p independently. This mixer uses a round belt instead of the miter gears so that we can rotate a larger container.

change Ω_s and Ω_p independently. More concretely, let Ω_u and Ω_l denote the rotation speeds of the upper and lower motors shown in Fig. 7(b), respectively. Then, the precession rotation speed Ω_p coincides with Ω_l. Since the miter rotates at $|\Omega_u - \Omega_l|$ with respect to the precession frame, the spin rotation speed is also $\Omega_s = |\Omega_u - \Omega_l|$. Thus, $Po = \Omega_l/|\Omega_u - \Omega_l|$ is controllable by changing Ω_u and Ω_l. However, the size of the container is limited by the size of the miter gears.

Next, we developed the third type of mixer [Fig. 7(c)] so that we could rotate larger containers. The driving mechanism is similar to the mixer in Fig. 7(b), but we use a round belt instead of a pair of miter gears to drive the spin. This enables us to use larger containers. However, because of the slip of the round belt for high rotation speeds, it was difficult to control Ω_s accurately.

Through preliminary experiments by these prototype mixers, we realized that it is important to conduct a systematic parameter survey with changing Ω_s, Ω_p, and the container's size before practical applications. In particular, for the high-shear-rate mixing, such as emulsification, we need to examine wide ranges of rotation speeds both for the spin Ω_s and precession Ω_p. The mixer (Fig. 2) used in the present experiments realizes this. Since the moment of inertia of the large aluminum drum is large enough to stabilize its rotation, i.e., $\boldsymbol{\Omega}_p$, we can conduct experiments with sufficiently high values of *Po*, which is required for effective mixing.

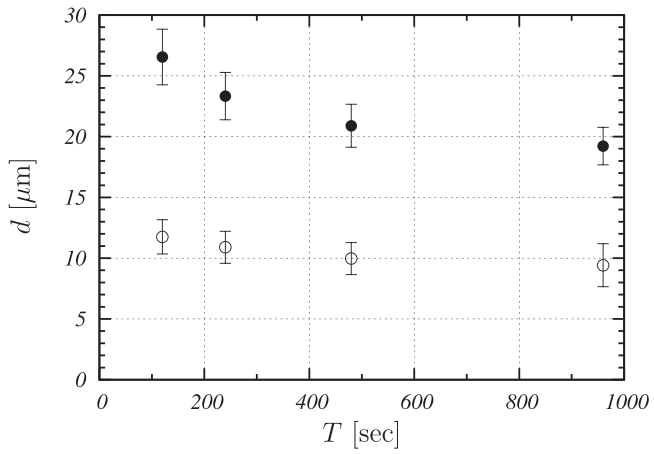

FIG. 8. Representative diameter *d* of oil droplets as a function of mixing time *T*. We use container D58L52, and the mixing parameters are $Po = 0.2$ and $\Omega_s = 2000$ rpm (•) and $Po = 0.2$ and $\Omega_s = 3000$ rpm (○).

APPENDIX B: DEPENDENCE ON MIXING TIME

In this appendix, we examine the mixing-time dependence of the size of produced droplets. We show in Fig. 8 the representative size of droplets produced in container D58L52. We fix $Po = 0.2$ and show two series of results with changing the mixing time T for $\Omega_s = 2000$ rpm (closed circles) and 3000 rpm (open circles). Though we observe that the droplet size decreases with T, the difference in the results with $T = 480$ s and 960 s is within the uncertainty of the measurements. This is the reason why we fix the mixing time T at 480 s in all the results for $Po = 0.2$ and 0.3 shown in Sec. III.

It is of importance to point out that the appropriate mixing time T depends on *Po*. This is because if we increase *Po* above the range ($Po = 0.2$–0.3) examined in the main text, the flow in the bulk becomes very quiescent. To show this property, we show in Fig. 9(a) the results obtained with D58L52 at spin rotation speed $\Omega_s = 1500$ rpm. The closed circles denote results with a fixed mixing time $T = 480$ s and changing *Po* in the range of $0.2 \leq Po \leq 0.8$. It is evident that the mixing time $T = 480$ s is not enough for the larger *Po*. Despite higher shear rates for $Po = 0.8$ than 0.6 (see Fig. 17 in Ref. 4 for the evidence that the shear rate is an increasing function of *Po* in the precessing sphere), the produced droplets are coarser. This property is more evident in Fig. 9(b), where we show the images of produced emulsion for $Po = 0.2$ and 0.8. Looking at the results for $Po = 0.8$, we can see that the mixing time $T = 240$ s is too short to produce the emulsion, and if we increase T up to 960 s, the produced droplets get finer than those for $Po = 0.2$ with the same mixing time. We can quantitatively confirm this in Fig. 9(a), where we plot results with $T = 960$ s by open circles. Incidentally, if we further increase T (1980 s) with $Po = 0.8$, we may produce even finer droplets [the blue square in Fig. 9(a)]. These results mean that, for practical mixing with a finite time, $Po = 0.2$–0.3 is reasonable for the combination of good mixing in the bulk and emulsification in the thin boundary layer.

APPENDIX C: VALIDATION OF THE DROPLET DIAMETER MEASUREMENT

In the present study, we estimate the representative diameter *d* of droplets in emulsion by measuring their rising velocity *V*. To validate this simple method under the bold assumption that *V* is

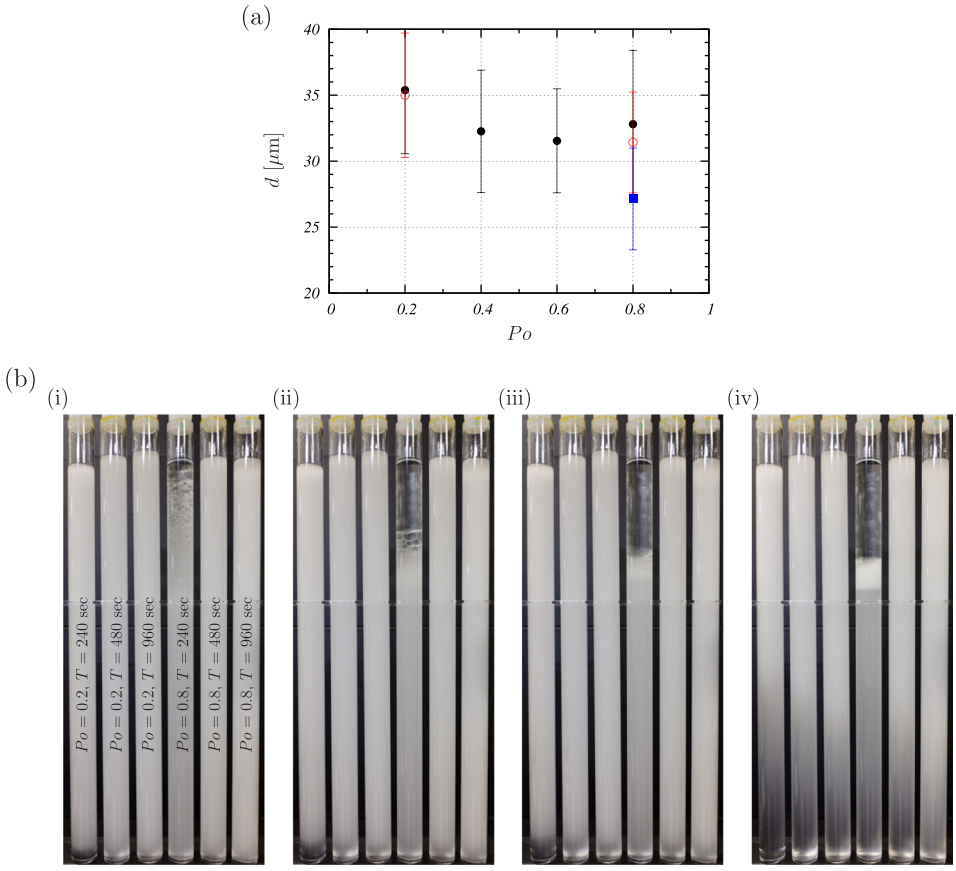

FIG. 9. (a) Similar to Fig. 4, but we fix the spin rotation speed at $\Omega_s = 1500$ rpm and we examine a wider range of Po. We use container D58L52. Different symbols show results with different mixing times: •—$T = 480$ s; ○—960 s; ■—1920 s. (b) The images of emulations for the two values of $Po = 0.2$ and 0.8 with three mixing times $T = 240$, 480, and 960 s. The images are taken at (i) 0, (ii) 1, (iii) 2, and (iv) 30 min after shaking by hands.

approximated by Eq. (3), we measure the diameter distribution of droplets by the laser diffraction method (Horiba, LA920). Since the Sauter mean diameter d_{32} is often used for the estimation of droplet size in emulsion,[29] we compare d with d_{32} in Fig. 10 for five different mixing conditions. It is evident in this figure that d and d_{32} are proportional to each other.

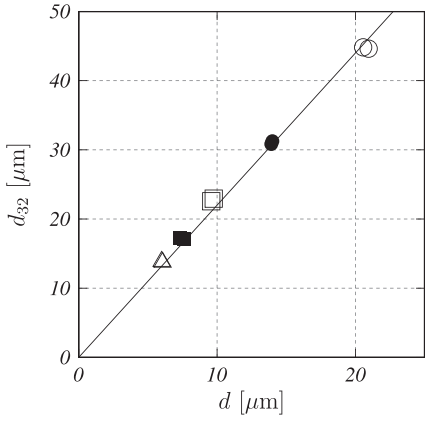

FIG. 10. Proportionality between the representative droplet diameter d measured by our method and the Sauter diameter d_{32} measured by the laser diffraction method. Emulsion is produced in container D58L52 with $Po = 0.3$. Different symbols denote results with different values of Ω_s: ○—2000; •—2500; □—3000; ■—3500; △—4000 rpm. The solid line indicates $d_{32} = 2.2d$.

REFERENCES

[1]H. P. Greenspan, *The Theory of Rotating Fluids* (Cambridge University Press, 1968).
[2]P. Meunier, "Geoinspired soft mixers," J. Fluid Mech. **903**, A15 (2020).
[3]D. Watanabe and S. Goto, "Simple bladeless mixer with liquid–gas interface," Flow **2**, E28 (2022).
[4]S. Goto, M. Shimizu, and G. Kawahara, "Turbulent mixing in a precessing sphere," Phys. Fluids **26**, 115106 (2014).
[5]S. Goto, N. Ishii, S. Kida, and M. Nishioka, "Turbulence generator using a precessing sphere," Phys. Fluids **19**, 061705 (2007).
[6]S. Goto, A. Matsunaga, M. Fujiwara, M. Nishioka, S. Kida, M. Yamato, and S. Tsuda, "Turbulence driven by precession in spherical and slightly elongated spheroidal cavities," Phys. Fluids **26**, 055107 (2014).
[7]F. H. Busse, "Steady fluid flow in a precessing spheroidal shell," J. Fluid Mech. **33**, 739–751 (1968).
[8]R. R. Kerswell, "On the inertial shear layer spawned by critical regions in oscillatory Ekman boundary layers," J. Fluid Mech. **298**, 311–325 (1995).
[9]J. Noir, D. Jault, and P. Cardin, "Numerical study of the motions within a slowly precessing sphere at low Ekman number," J. Fluid Mech. **437**, 282–299 (2001).
[10]S. Kida, "Steady flow in a rapidly rotating sphere with weak precession," J. Fluid Mech. **680**, 150–193 (2011).
[11]S. Kida, "Steady flow in a rapidly rotating spheroid with weak precession—Part 1," Fluid Dyn. Res. **52**, 015513 (2020).
[12]S. Kida, "Steady flow in a rapidly rotating spheroid with weak precession—Part 2," Fluid Dyn. Res. **53**, 025501 (2021).

[13]R. Manasseh, "Breakdown regimes of inertia waves in a precessing cylinder," J. Fluid Mech. **243**, 261–296 (1992).
[14]A. Tilgner and F. H. Busse, "Fluid flows in precessing spherical shells," J. Fluid Mech. **426**, 387–396 (2001).
[15]R. Hollerbach, C. Nore, P. Marti, S. Vantieghem, F. Luddens, and J. Léorat, "Parity-breaking flows in precessing spherical containers," Phys. Rev. E **87**, 053020 (2013).
[16]Y. Lin, P. Marti, and J. Noir, "Shear-driven parametric instability in a precessing sphere," Phys. Fluids **27**, 046601 (2015).
[17]J. Vormann and U. Hansen, "Numerical simulations of bistable flows in precessing spheroidal shells," Geophys. J. Int. **213**, 786–797 (2018).
[18]C. Nobili, P. Meunier, B. Favier, and M. Le Bars, "Hysteresis and instabilities in a spheroid in precession near the resonance with the tilt-over mode," J. Fluid Mech. **909**, A17 (2021).
[19]F. Pizzi, A. Giesecke, J. Šimkanin, and F. Stefani, "Prograde and retrograde precession of a fluid-filled cylinder," New J. Phys. **23**, 123016 (2021).
[20]W. V. R. Malkus, "Precession of the earth as the cause of geomagnetism," Science **160**, 259–264 (1968).
[21]J. Vanyo, P. Wilde, P. Cardin, and P. Olson, "Experiments on precessing flows in the Earth's liquid core," Geophys. J. Int. **121**, 136–142 (1995).
[22]P. Meunier, C. Eloy, R. Lagrange, and F. Nadal, "A rotating fluid cylinder subject to weak precession," J. Fluid Mech. **599**, 405–440 (2008).
[23]M. Le Bars, D. Cébron, and P. Le Gal, "Flows driven by libration, precession, and tides," Ann. Rev. Fluid Mech. **47**, 163–193 (2015).
[24]D. Cébron, R. Laguerre, J. Noir, and N. Schaeffer, "Precessing spherical shells: Flows, dissipation, dynamo and the lunar core," Geophys. J. Int. **219**, S34–S57 (2019).
[25]K. Komoda and S. Goto, "Three-dimensional flow structures of turbulence in precessing spheroids," Phys. Rev. Fluids **4**, 014603 (2019).
[26]K. Matsuyama, K. Mine, H. Kubo, N. Aoki, and K. Mae, "Optimization methodology of operation of orifice-shaped micromixer based on micro-jet concept," Chem. Eng. Sci. **65**, 5912–5920 (2010).
[27]S. Kida, "Steady flow in a rotating sphere with strong precession," Fluid Dyn. Res. **50**, 021401 (2018).
[28]F. Pizzi, A. Giesecke, and F. Stefani, "Ekman boundary layers in a fluid filled precessing cylinder," AIP Adv. **11**, 035023 (2021).
[29]S. Middleman, "Drop size distributions produced by turbulent pipe flow of immiscible fluids through a static mixer," Ind. Eng. Chem. Process Des. Dev. **13**, 78–83 (1974).